Developmental Biology 442 (2018) 199–209

Contents lists available at ScienceDirect

Developmental Biology

journal homepage: www.elsevier.com/locate/developmentalbiology

Short Communication

# Developmental SMAD6 loss leads to blood vessel hemorrhage and disrupted endothelial cell junctions

Lyndsay A. Wylie[a], Kevin P. Mouillesseaux[e], Diana C. Chong[f], Victoria L. Bautch[a,b,c,d,*]

[a] Curriculum in Genetics and Molecular Biology, The University of North Carolina at Chapel Hill, Chapel Hill, NC 27599, USA
[b] Department of Biology, The University of North Carolina at Chapel Hill, Chapel Hill, NC 27599, USA
[c] Lineberger Comprehensive Cancer Center, The University of North Carolina at Chapel Hill, Chapel Hill, NC 27599, USA
[d] McAllister Heart Institute, The University of North Carolina at Chapel Hill, Chapel Hill, NC 27599, USA
[e] StrideBio, Inc., Durham, NC 27701, USA
[f] Dept. of Medicine, Duke University, Durham, NC 27710, USA

ARTICLE INFO

*Keywords:*
SMAD6
Angiogenesis
Mouse development
Retina
VE-cadherin

ABSTRACT

The BMP pathway regulates developmental processes including angiogenesis, yet its signaling outputs are complex and context-dependent. Recently, we showed that SMAD6, an intracellular BMP inhibitor expressed in endothelial cells, decreases vessel sprouting and branching both *in vitro* and in zebrafish. Genetic deletion of SMAD6 in mice results in poorly characterized cardiovascular defects and lethality. Here, we analyzed the effects of SMAD6 loss on vascular function during murine development. SMAD6 was expressed in a subset of blood vessels throughout development, primarily in arteries, while expression outside of the vasculature was largely confined to developing cardiac valves with no obvious embryonic phenotype. Mice deficient in SMAD6 died during late gestation and early stages of postnatal development, and this lethality was associated with vessel hemorrhage. Mice that survived past birth had increased branching and sprouting of developing postnatal retinal vessels and disorganized tight and adherens junctions. *In vitro*, knockdown of SMAD6 led to abnormal endothelial cell adherens junctions and increased VE-cadherin endocytosis, indicative of activated endothelium. Thus, SMAD6 is essential for proper blood vessel function during murine development, where it appears to stabilize endothelial junctions to prevent hemorrhage and aberrant angiogenesis.

## 1. Introduction

Angiogenesis, the growth of new blood vessels from pre-existing vessels, is essential for proper development, as the cardiovascular system is the first to form and function during embryogenesis (Risau, 1997; Carmeliet, 2003). For angiogenesis to occur, endothelial cells (EC) must initiate a multi-stage program of basement membrane degradation, polarity switching, proliferation, and migration into the surrounding matrix (Adams and Alitalo, 2007; Geudens and Gerhardt, 2011). Perturbations of angiogenic pathways during development often lead to early embryonic lethality.

Proper angiogenesis requires that EC establish and modify cell-cell interactions with neighboring EC. Several types of EC junctions are involved in blood vessel expansion, including tight and adherens junctions, and modulation of adherens junctions is a critical first step in new blood vessel formation (Dejana et al., 2009; Wallez and Huber, 2008). VE-cadherin is a key component of EC adherens junctions, and homotypic binding between VE-cadherin molecules on adjacent EC sets up cell-cell interactions (Vestweber et al., 2009). Adherens junctions are involved in junction remodeling in sprouting vessels and aid in junction stabilization of large vessels, such as the developing aorta (Giannotta et al., 2013). Endothelial cell-cell interactions also regulate vascular permeability and barrier function, and disruption of EC junctions results in increased EC permeability, often leading to edema and hemorrhage (Dejana et al., 2009; Curry and Adamson, 2010; Komarova et al., 2017; Corada et al., 1999).

Bone Morphogenetic Protein (BMP) signaling regulates angiogenesis, with certain pathway components either promoting or inhibiting angiogenesis (Cai et al., 2012; David et al., 2009). In canonical signaling, BMP ligands bind cell-surface Type II and Type I receptors that form heterotetrameric complexes. Phosphorylation of Type I receptors by Type II receptors triggers phosphorylation of receptor associated SMADs (R-SMADs), which in BMP signaling are SMADs 1, 5, and 8 (Shi and Massague, 2003). R-SMADs then bind to a common SMAD, SMAD4, and translocate into the nucleus to regulate the expression of target genes (Derynck and Zhang, 2003; Bragdon et al., 2011).

* Correspondence to: Department of Biology, CB#3280, University of North Carolina at Chapel Hill, Chapel Hill, NC 27599, USA.
*E-mail address:* bautch@med.unc.edu (V.L. Bautch).

https://doi.org/10.1016/j.ydbio.2018.07.027
Received 5 April 2018; Received in revised form 13 July 2018; Accepted 31 July 2018
Available online 09 August 2018

BMP-induced sprouting *via Bmp2b* in zebrafish is exclusive to the caudal vein plexus and absent in the dorsal aorta (DA) during development (Wiley et al., 2011). BMP signaling also promotes angiogenesis in Human Umbilical Vein Endothelial Cells (HUVEC), as BMP2 and BMP6 ligands increase lateral vessel branching (Mouillesseaux et al., 2016). In contrast, BMP9 functions as an anti-angiogenic signal, inducing quiescent EC and mature networks lacking growth features (David et al., 2007; Larrivee et al., 2012; Ricard et al., 2012). Both pro- and anti-angiogenic BMP signaling are important in sprouting angiogenesis in the early postnatal retina. Vascular deletion of either the Type II receptor BMPR2 or the Type I receptors Alk2/ACVR1 or Alk3/BMPR1A leads to reduced sprouting and/or branching, while vascular deletion of Alk1 leads to excess sprouting (Lee et al., 2017). Although BMP signaling in the vasculature is considered to be "context-dependent", it is not clear at the molecular level why some vessels respond to BMP signals with sprouting angiogenesis, while others do not.

Numerous cell extrinsic negative regulators of BMP influence signaling, but there are few identified cell-intrinsic negative regulators of BMP signaling (Smith, 1999; Miyazawa and Miyazono, 2017). SMAD6 is one such cell-intrinsic negative regulator of BMP signaling expressed in EC (Hata et al., 1998; Imamura et al., 1997). We recently showed that SMAD6 is anti-angiogenic in an *in vitro* 3D angiogenesis assay and *in vivo* in zebrafish (Mouillesseaux et al., 2016). Mice globally lacking *Smad6* primarily die embryonically and perinatally, surviving mice exhibit cardiovascular defects and hypertension (Galvin et al., 2000), and SMAD6 is also required for endochondral bone formation (Estrada et al., 2011). However, it is unclear how loss of *Smad6* affects murine embryonic vascular development and angiogenesis.

Here we investigated the role of SMAD6 in developing murine blood vessels, and identify a novel role for SMAD6 in vessel stability associated with changes in EC junctions *in vivo* and *in vitro*. We found that mouse embryos lacking *Smad6* function displayed hemorrhage, suggesting increased vessel permeability. SMAD6 expression was localized to a subset of vessels developmentally, with limited non-vascular expression, and *Smad6* loss resulted in increased sprouting and branching in the early postnatal retina, accompanied by mis-localization of the junction proteins VE-cadherin and ZO-1. These results point to a previously unappreciated role for SMAD6 in developmental angiogenesis, with effects on both sprouting and vessel stability that likely account for some of the context-dependent outputs of BMP signaling in the vasculature.

## 2. Results

### 2.1. Loss of Smad6 is lethal with moderate penetrance and vessel hemorrhage

Global loss of *Smad6* results in embryonic and postnatal lethality with moderate penetrance (Galvin et al., 2000; Estrada et al., 2011). Surviving adult mice have hyperplastic thickening of the cardiac valves, defects in outflow tract septation, and hypertension (Galvin et al., 2000). To begin our studies of SMAD6 function in developing vessels, we analyzed the genotypes of progeny of a *Smad6*$^{+/-}$ intercross at P0 **(**Table 1**)** and found significantly fewer *Smad6*$^{-/-}$ mutant mice than expected, suggesting embryonic lethality with partial penetrance. Of the mutant mice that survived to birth, most of these died within 2–6 days of birth (data not shown). Because surviving adult *Smad6*$^{-/-}$ mutant mice were reported to have heart valve defects (Galvin et al., 2000), we examined H & E stained sections of heart valves at embryonic day (E)15.5 and postnatal day (P)3 and found no evidence of hyperplastic thickening or other defects **(**Fig. 1**A–F)**, suggesting that heart defects are not the cause of embryonic lethality in *Smad6* mutant mice. The valve phenotype previously described was documented in post-natal and adult mice on a different genetic background, which may account for the differences. We next broadly examined the embryonic vasculature *via* light-sheet microscopy, using a PECAM antibody to visualize all blood vessels. We saw no obvious gross vascular patterning changes in E15.5 *Smad6*$^{-/-}$ mutant embryos, suggesting that if sprouting angiogenesis is affected, remodeling subsequent to sprouting may rescue any initial defects **(**Fig. 1**G–J)**. Further examination of mutant embryos revealed areas of hemorrhage, which could be seen as early as E12.5 (data not shown) and were consistent by E15.5 **(**Fig. 1**K–L)**. Hemorrhage was noted at multiple locations in the mutant embryos, including in the skin **(**Fig. 1**M–N)** and in brown fat pads **(**Fig. 1**O–P).** We quantified the hemorrhage in E15.5 wildtype and *Smad6*$^{-/-}$ embryos *via* Prussian Blue staining and found significantly more hemorrhage in Smad6$^{-/-}$ embryos **(**Fig. 1**Q–S)**. Collectively, these results indicate that *Smad6* deletion leads to hemorrhage of embryonic vessels in the absence of obvious patterning defects. Since hemorrhage often results in lethality, we propose that the observed embryonic and early postnatal lethality is downstream of vascular hemorrhage.

**Table 1**
Underrepresentation of *Smad6*$^{-/-}$ mice at P0.

| P0 Mice (total = 133 (100%)) | | | | | |
|---|---|---|---|---|---|
| ***Smad6*$^{+/+}$** | | ***Smad6*$^{+/-}$** | | ***Smad6*$^{-/-}$**$^{**}$ | |
| **Observed** | **Expected** | **Observed** | **Expected** | **Observed** | **Expected** |
| 46 (35%) | 33 (25%) | 76 (57%) | 67 (50%) | 11 (8%) | 33 (25%) |

$\chi^2 = 13.71$, df = 2, ** $P = < 0.0011$ for *Smad6*$^{-/-}$ P0 mice, observed vs. expected.

### 2.2. SMAD6 is selectively expressed in a subset of vessels developmentally

The embryonic vascular hemorrhage phenotype in the absence of obvious non-vascular defects in *Smad6*$^{-/-}$ mutant mice suggested that SMAD6 expression may be primarily localized to developing blood vessels during mouse development. Earlier studies showed SMAD6 expression in the cardiac outflow tract and dorsal aorta, the atrioventricular cushion, cardiac valves, and in the cartilage and ribs of embryos (Galvin et al., 2000; Estrada et al., 2011). We examined expression using the *LacZ* knock-in reporter in the locus as a surrogate for SMAD6 expression in the *Smad6*$^{-/-}$ background, since we did not see gross vessel patterning defects in the mutant embryos. *LacZ* expression was detected in the heart and cardiac outflow tract at E9.5 **(**Fig. 2**A).** At E10.5, as the dorsal aorta begins to stabilize, *LacZ* was expressed in the heart and dorsal aorta **(**Fig. 2**B–C)**. At E13.5, 15.5 and 17.5, *LacZ* expression was seen in the descending aorta and in intercostal arteries emanating from the aorta in *Smad6*$^{-/-}$ embryos **(**Fig. 2**D, E, G),** while *LacZ* expression was not detectable in these vessels in *Smad6*$^{+/+}$ embryos **(**Fig. 2**F).** At E13.5–15.5, *LacZ* expression was detected in the branchial arch arteries, including the common carotid arteries and the left and right subclavian arteries **(**Fig. 2**D, H),** and in vessels in the embryonic head **(**Fig. 2**I).** Further analysis of the postnatal brain (P3) showed strong expression in conduit arteries such as the middle cerebral artery **(**Fig. 2**J–K)** and basilar artery **(**Fig. 2**J).** The restricted vascular expression of the *Smad6* reporter was revealed by comparison to brains of P3 mice expressing *LacZ* from the *Flt1* locus, which is expressed in all or most vessels, including veins and capillaries (Compare Fig. 2**K** and **L**). Sections of *Smad6*$^{-/-}$ β-gal-stained embryos revealed reporter expression localized to the inner layer of the dorsal aorta and in smaller arteries throughout the embryo, including the vertebral and postnatal brain vessels **(**Fig. 2**M–P),** but not in the cartilage of the tibia **(**Fig. 2**Q).** At E15.5, reporter expression from the *Smad6* locus was also detected in the outflow tract of the heart, but not in non-vascular tissue of other embryonic organs such as lungs, pancreas, stomach, and kidney **(**Fig. 2**R–U)**. To determine which vascular cells express SMAD6, serial sections of E15.5 embryos

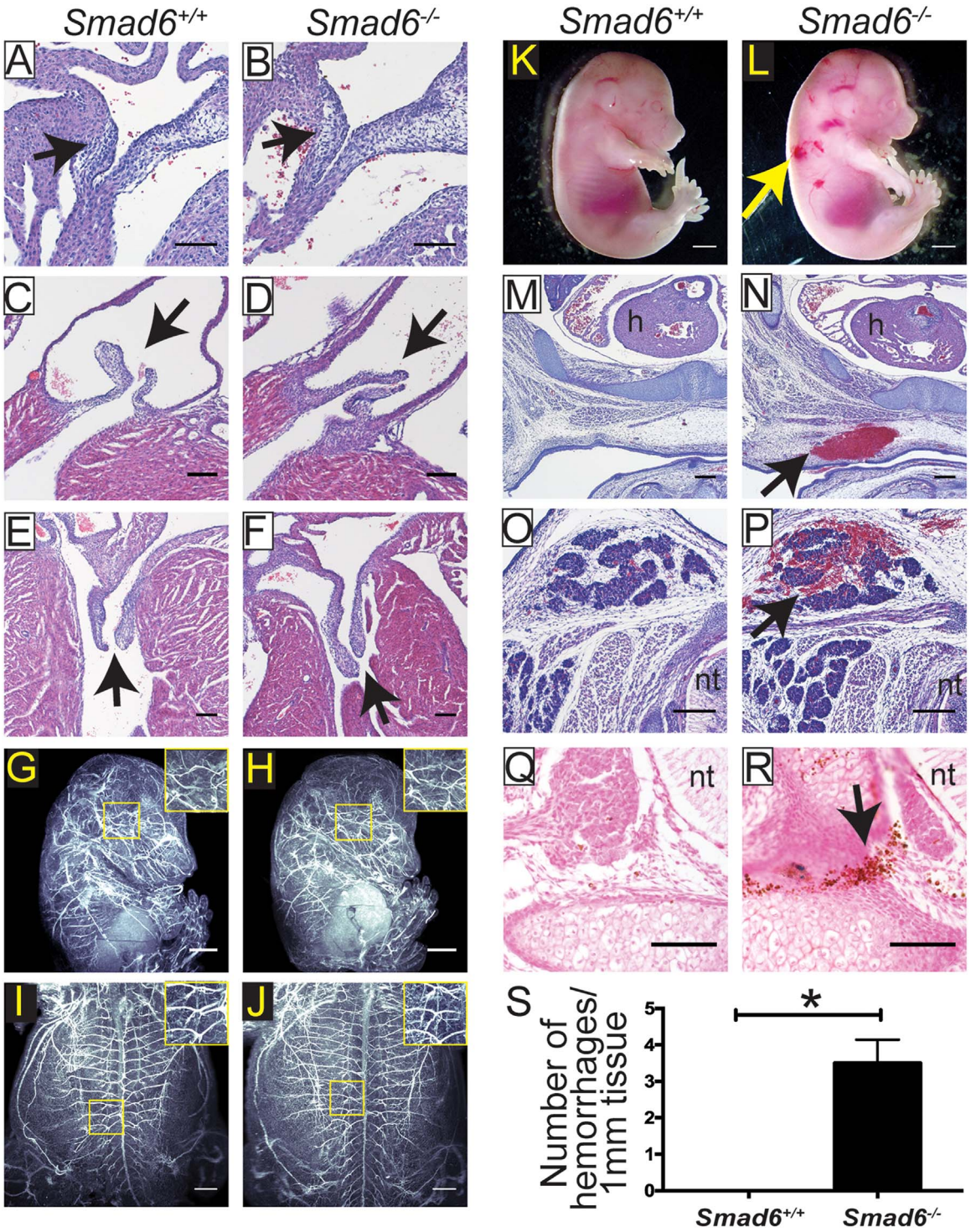


**Fig. 1. Loss of SMAD6 results in embryonic vessel hemorrhage at E15.5. A–B,** 10 μm paraffin sections of E15.5 heart valve primordia of indicated genotypes stained with Hematoxylin and Eosin (H & E). Arrow, valve primordium; scale bar, 100 μm. **C–F,** 10 μm paraffin sections of P4 pulmonary **(C–D)** and mitral **(E–F)** valves of indicated genotypes stained with H & E. Arrow, valve; scale bar, 100 μm. **G–J,** Whole mount E15.5 embryos of indicated genotypes stained with PECAM to visualize blood vessels and imaged using light-sheet microscopy. **G–H**, lateral view; **I–J**, ventral view. Higher magnification insets reveal no significant vessel patterning differences between *Smad6*$^{+/+}$ **(G, I)** and *Smad6*$^{-/-}$ **(H, J)** embryos. Scale bar, G–H, 1000 μm, I–J, 500 μm. **K–L,** E15.5 whole mount embryos showing hemorrhage in *Smad6*$^{-/-}$ embryo (**L,** arrow, hemorrhage); scale bar, 1000 μm. **M–P,** Sections through 2 different E15.5 *Smad6*$^{+/+}$ **(M, O)** and *Smad6*$^{-/-}$ **(N, P)** embryos showing hemorrhage (arrow in **N, P**), stained with H & E; scale bar, 200 μm. h, heart; nt, neural tube. **Q–R,** Prussian Blue-DAB on E15.5 embryo sections used for quantification in Fig. 1**S.** (**R**, arrow, hemorrhage); scale bar, 100 μm. nt, neural tube. **S**, Quantification of hemorrhage per mm of embryonic tissue. *, $P \leq 0.05$, statistical significance was assessed using a Student's *t*-test, Mann-Whitney *post-hoc* test, 4 replicates.

and postnatal brains (P3) were stained with either X-gal or antibodies to PECAM-1 (EC marker), α-SMA (smooth muscle marker), and NG2 (pericyte marker/smooth muscle marker). *Smad6 LacZ* reporter expression co-localizes to EC and does not overlap with α-SMA or NG2 staining **(**Fig. 2**V–V”” and W–W””)**.

Taken together, these results indicate that SMAD6 is expressed in the EC of a subset of vessels during mouse development, and expression was not detectable in other tissues or cell types except for the heart, consistent with the vascular phenotype that was observed in *Smad6*$^{-/-}$ mutant embryos. Moreover, most of the vascular expression

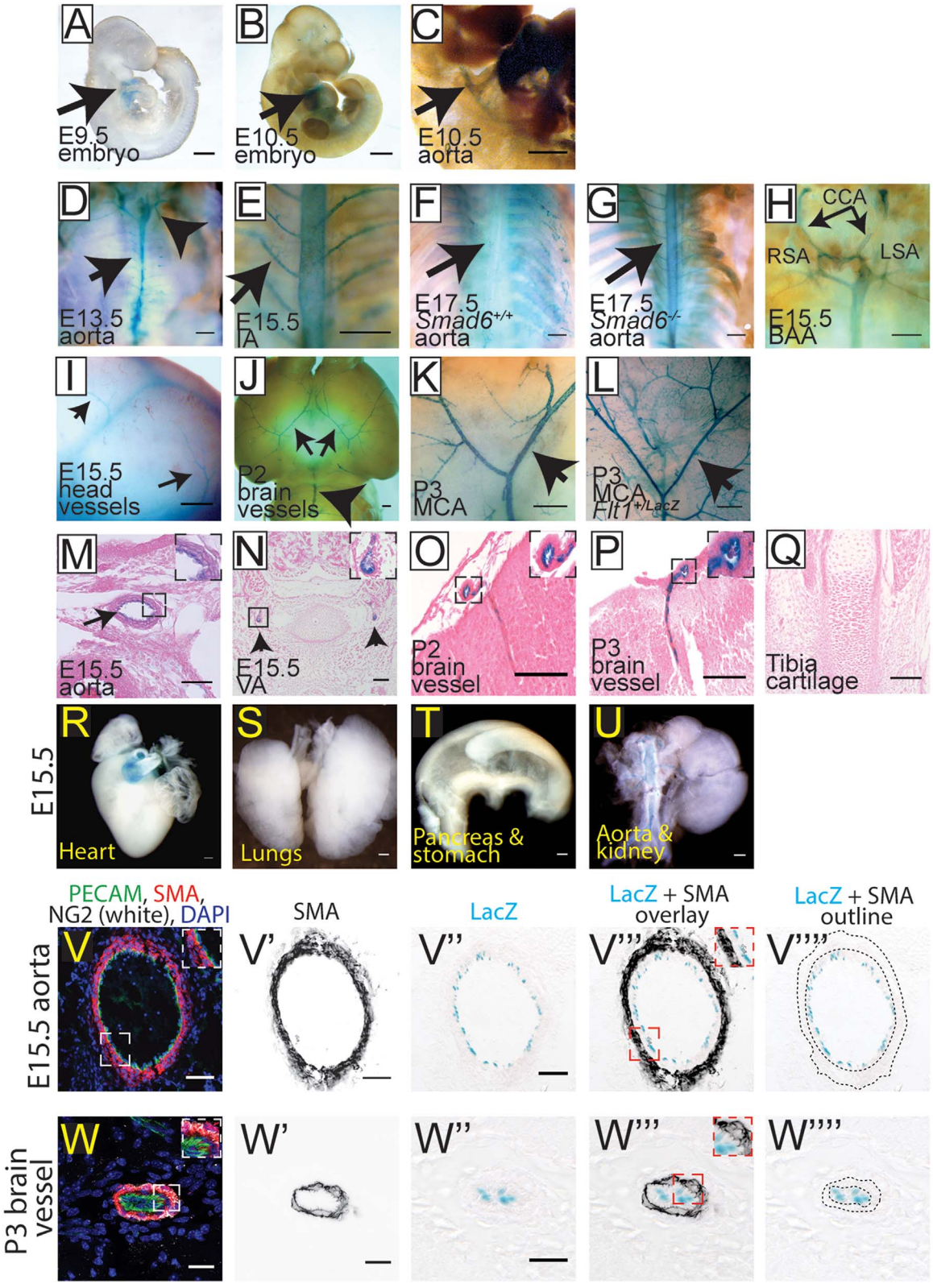
A
E9.5 embryo
B
E10.5 embryo
C
E10.5 aorta
D
E13.5 aorta
E
E15.5 IA
F
E17.5 Smad6+/+ aorta
G
E17.5 Smad6-/- aorta
H
CCA
RSA
LSA
E15.5 BAA
I
E15.5 head vessels
J
P2 brain vessels
K
P3 MCA
L
P3 MCA Flt1+/LacZ
M
E15.5 aorta
N
E15.5 VA
O
P2 brain vessel
P
P3 brain vessel
Q
Tibia cartilage
E15.5
R
Heart
S
Lungs
T
Pancreas & stomach
U
Aorta & kidney
PECAM, SMA, NG2 (white), DAPI
SMA
LacZ
LacZ + SMA overlay
LacZ + SMA outline
E15.5 aorta
V
V'
V''
V'''
V''''
P3 brain vessel
W
W'
W''
W'''
W''''

**Fig. 2. SMAD6 is selectively expressed in a subset of vessels developmentally. A–L,** Whole embryos stained for *LacZ* expression (blue). **M–Q,** cross sections of embryos stained for *LacZ* expression, counterstained with eosin (pink). **A,** E9.5 embryo with *LacZ* expression in the heart and outflow tract (arrow, heart). **B–C,** E10.5 embryo showing *LacZ* expression in heart and dorsal aorta (DA) (arrows, DA). **C)** Higher magnification of DA staining in **(B). D–G,** Body cavities of E13.5 *Smad6*$^{-/-}$ **(D)**, E15.5 *Smad6*$^{-/-}$ **(E)**, and E17.5 *Smad6*$^{+/+}$ **(F)** and *Smad6*$^{-/-}$ **(G)** embryos with all organs removed to show *LacZ* expression in aorta (black arrows in **D, G**) and intercostal arteries (IA) (arrow in **E**), compared to only background in *Smad6*$^{+/+}$ embryo **(F)** (Arrowhead in **D**, branchial arch arteries). **H,** E15.5 *Smad6*$^{-/-}$ branchial arch arteries (BAA) positive for *LacZ* expression. CCA, common carotid arteries; LSA, left subclavian artery; RSA, right subclavian artery. **I,** Blood vessels expressing *LacZ* in E15.5 *Smad6*$^{-/-}$ embryo head (arrows, vessels). **J–K,** Postnatal (P2–3) *Smad6*$^{-/-}$ brains showing arterial *LacZ* expression. MCA, Middle cerebral arteries; BA, basilar artery (arrows **J–K**, MCA; arrowhead **J,** BA). **L,** *Flt1*$^{+/LacZ}$ P3 brain showing arterial, venous, and capillary *LacZ* expression; arrow to MCA. **M,** Cross-section showing *LacZ* expression in aorta of E15.5 *Smad6*$^{-/-}$ embryo (arrow, aorta); inset, higher magnification of aorta. **N,** E15.5 *Smad6*$^{-/-}$ embryo cross-section with staining in smaller vertebral arteries (arrows, vertebral arteries); inset, higher magnification of left vertebral artery. **O–P,** Cross-sections of postnatal (P2–3) brains; insets, higher magnification of indicated vessel. **Q,** Cross-section of E15.5 tibia cartilage showing no detectable *LacZ* expression. **R–U,** Whole mount of indicated E15.5 organs stained for *LacZ* expression. *LacZ* expression is detected in the outflow tract of the heart **(R)**, but not in non-vascular tissue of lungs **(S)**, stomach and pancreas **(T)**, or kidney (**U**, note *LacZ* expression in aorta connected to kidney). **V–W"",** E15.5 *Smad6*$^{-/-}$ aorta (**V–V""**) and P3 brain (**W–W""**) serial cross-sections stained with α-smooth muscle actin (SMA, red), PECAM (green), NG2 (white) and DAPI (blue) in V, W. **V', W',** SMA channel alone. **V", W",** *LacZ* reporter expression (blue) in same cross-section as in V' and W'. **V'"–W'",** proportional overlay of SMA and *LacZ* expression patterns (compare insets in V, W to insets in V'", W'"). **V"", W"",** SMA layer outline (dotted lines) over *LacZ* expression image, showing no apparent overlap between SMA and *LacZ* (SMAD6) expression. Scale bars: A–I, 500 μm; J–L, R–U, 1000 μm; M–Q, 100 μm; V–V"", 50 μm; W–W"", 20 μm.

appears confined to developing arteries, and most veins and capillaries do not have detectable levels of reporter expression. Thus, the embryonic vascular hemorrhage phenotype observed in the *Smad6*$^{-/-}$ mutant mice is likely due to primary defects in these vessels.

### 2.3. SMAD6 prevents excessive sprouting and branching in retinal vessels

To examine *Smad6* function during sprouting angiogenesis in developing vessels that are known to respond to manipulations of BMP signaling (Lee et al., 2017), we analyzed the postnatal retinal vasculature in pups that survived birth **(**Table 1**)**. Smad6 RNA is expressed in retinas of wildtype P4 pups, with significantly reduced levels in *Smad6*$^{+/-}$ heterozygous and *Smad6*$^{-/-}$ mutant pups **(**Fig. 3**A)**. Retinal vessels develop by spreading radially from the optic nerve over the surface of the retina, starting at P0. Vessels closer to the to the optic nerve undergo remodeling and become more stable and quiescent, whereas vessels at the vascular front are newly formed (Fruttiger, 2007; Dorrell et al., 2002; Gerhardt et al., 2003). We hypothesized that in this area of robust sprouting angiogenesis, loss of *Smad6* would lead to increased vessel sprouting and branching. The retinal vasculature of P4 *Smad6*$^{-/-}$ mutant mice appeared denser compared to *Smad6*$^{+/+}$ littermate controls, but radial expansion was not compromised **(**Fig. 3**B–D),** indicating no developmental delay. Closer examination of the vascular front showed that *Smad6*$^{-/-}$ mutant retinas had significantly more sprouts than littermate controls **(**Fig. 3**E–G)**. *Smad6*$^{-/-}$ mutant mice also had significantly more branching in the plexus behind the vascular front, which is typically a more stable vascular bed **(**Fig. 3**H–J)**. In *Smad6*$^{-/-}$ mutant retinas, vessels were often found in several layers (note depth-encoded images Fig. 3**H–I**), suggesting a lack of normal quiescence and remodeling. Thus, SMAD6 is anti-angiogenic in the developing mouse retina.

### 2.4. SMAD6 promotes VE-cadherin localization and blunts internalization

The increased branching of *Smad6*$^{-/-}$ mutant vessels behind the vascular front suggested that these vessels did not undergo flow-mediated remodeling but rather continued to sprout. A hallmark of activated blood vessels is destabilized adherens junctions (Adams and Alitalo, 2007; Geudens and Gerhardt, 2011). Thus, we hypothesized that SMAD6 stabilizes EC adherens junctions, and we examined the localization of VE-cadherin, a major EC adherens junction protein, in the mutant retinal vessels. VE-cadherin localization is indicative of active (dispersed or serrated) or stabilized (straight line) junctions (Kametani and Takeichi, 2006; Bentley et al., 2014). In *Smad6*$^{+/+}$ littermate controls VE-cadherin localization was mainly linear at the cell membrane **(**Fig. 3**K, M)**; in contrast, *Smad6*$^{-/-}$ mutant retinas had a striking dispersed and punctate pattern of VE-cadherin **(**Fig. 3**L, N)**. Since adherens junction disruption is often upstream of tight junction defects in EC, we examined the localization of the tight junction protein ZO-1 in P4 retinas, and found a similar non-linear, punctate pattern in *Smad6*$^{-/-}$ mutant tissue **(**Fig. 3**O–R).** These results show that SMAD6 affects endothelial junctions *in vivo* and suggest that SMAD6 is upstream of stabilized junctions as blood vessels remodel.

To further examine and quantify the effects of SMAD6 manipulations on EC adherens junctions, we examined the effects of reduced SMAD6 levels on junctions formed in HUVEC on micropatterns designed to hold 2 cells side-by-side (Tseng et al., 2012). Western blot analysis confirmed significant SMAD6 knockdown **(**Fig. 4**A)**. HUVEC transfected with a non-targeting siRNA control (NT siRNA) showed predominantly linear VE-cadherin staining **(**Fig. 4**B, D)**, indicating that the junctions are likely stabilized. In contrast, HUVEC with reduced SMAD6 levels had a more serrated and/or punctate VE-cadherin pattern **(**Fig. 4**C–D)**, suggesting more active junctions and consistent with our hypothesis.

Increased active junctions are often associated with elevated VE-cadherin endocytosis, and signaling through BMP6 increases VE-cadherin internalization in EC (Gavard and Gutkind, 2006; Benn et al., 2016). To determine whether SMAD6 KD increases VE-cadherin internalization, we performed an internalization assay on HUVEC transfected with either NT or SMAD6 siRNA. We labeled VE-cadherin with a primary antibody (BV6) to the extracellular domain at 4 °C (Corada et al., 2001). We then allowed internalization to occur at 37 °C in the absence or presence of BMP6 ligand and with or without reduced SMAD6 levels. To distinguish between the cell surface and internalized pool of VE-cadherin, we removed the cell surface antibody with an acid wash, then fixed and stained the cells with a secondary antibody to VE-cadherin (green, Fig. 4**E–I, J–N**), phalloidin (red) and DRAQ7 (blue) (merged images shown in Fig. 4**E'–I', J'–N'**), and quantified the internalized VE-cadherin pool. Prior to acid wash, VE-cadherin was detected and localized at the cell surface, presumably in adherens junctions, as predicted **(**Fig. 4**E–E', J–J').** Control HUVEC kept at 4 °C to prevent internalization did not show detectable VE-cadherin staining after acid wash, suggesting that the antibody-labeled protein was not internalized and therefore susceptible to acid wash **(**Fig. 4**F–F', G–G', K–K', L–L').** Vehicle-treated HUVEC incubated at 37 °C showed increased intracellular VE-cadherin staining that increased significantly with BMP6 ligand incubation, suggesting VE-cadherin internalization **(**Fig. 4**H–H', I–I', O)**. SMAD6 siRNA treated HUVEC at 37 °C showed significant intracellular VE-cadherin staining in both control conditions and with addition of BMP6 **(**Fig. 4**M–M', N–N', O).** These results suggest that SMAD6 stabilizes endothelial cell-cell junctions and prevents VE-cadherin endocytosis.

## 3. Discussion

This work reveals a required role for the negative BMP regulator, SMAD6, during mouse vascular development. The phenotype of embryonic vessel hemorrhage and the restriction of SMAD6 expression to specific vessels in the embryo indicate that SMAD6 normally functions to stabilize vessels and prevent leak and hemorrhage. This

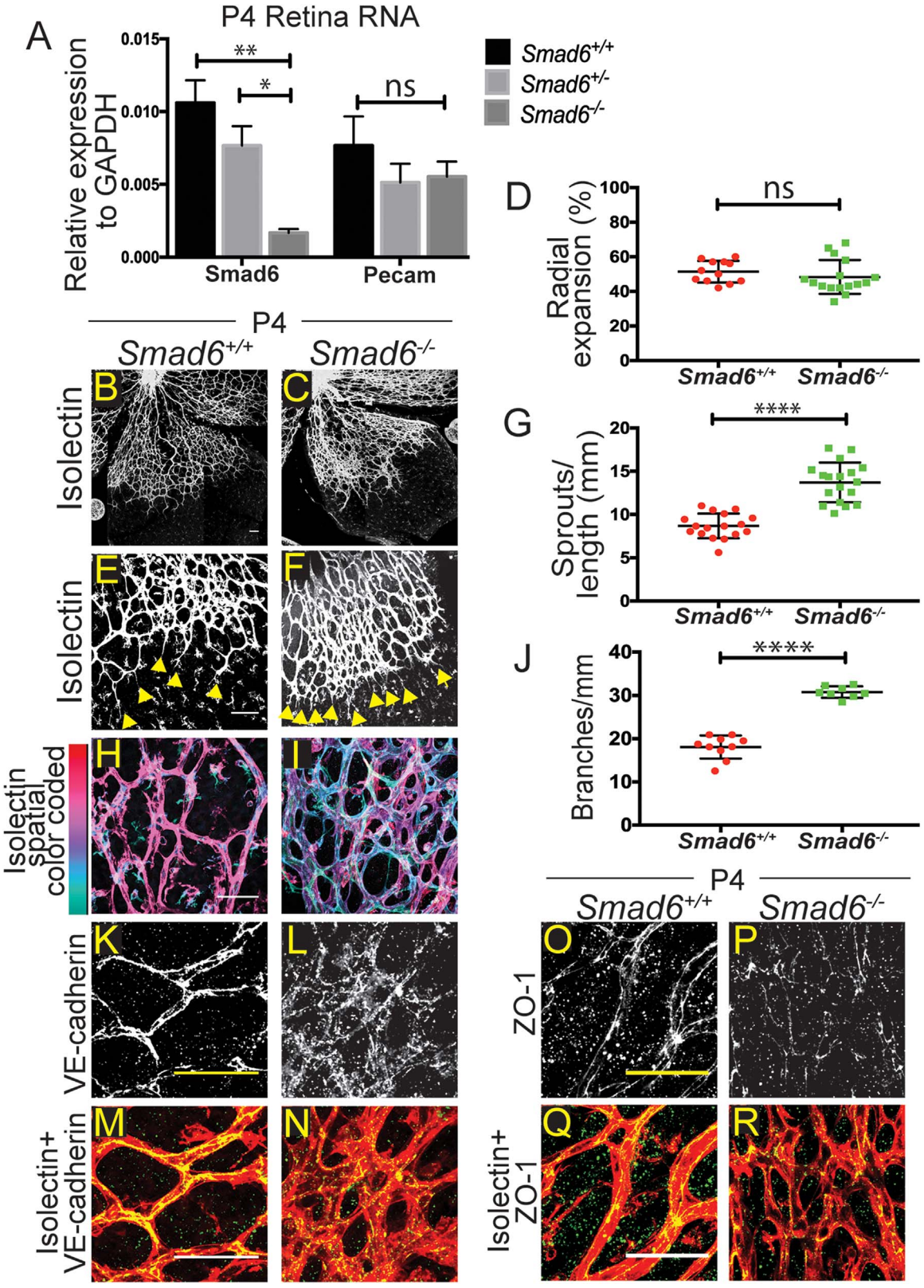


**Fig. 3. SMAD6 regulates postnatal retinal angiogenesis. A,** qRT-PCR for Smad6 RNA in P4 retinas of indicated genotypes. Pecam, positive control (3 replicates). **B–C,** P4 retinas stained with Isolectin-IB4 (white) to visualize vessels; **(B)** *Smad6*$^{+/+}$*and* **(C)** *Smad6*$^{-/-}$ littermates; scale bar, 100 μm. **D,** Quantification of radial expansion (% vessel length/ retina leaf length). ns, not significant. **E–F,** Examples of retinal vascular front of **(E)** *Smad*$^{+/+}$ and **(F)** *Smad6*$^{-/-}$ littermates (yellow arrows, sprout tips); scale bar, 100 μm. **G,** Quantification of sprouts (# sprouts/length of front). **H–I,** Examples of retinal vascular plexus region, stained for Isolectin, with Z-stacks depth-encoded for *Smad6*$^{+/+}$ **(H)** comparison to *Smad6*$^{-/-}$ littermates **(I)**; scale bar, 50 μm. **J,** Quantification of branching. **K–L,** Retinal vessels stained for VE-cadherin (white); scale bar, 50 μm. **M–N**, Merged images of K–L, VE-cadherin (green) and Isolectin (red); scale bar, 50 μm. *Smad6*$^{+/+}$ **(K, M)** and *Smad6*$^{-/-}$ **(L, N). O–P,** Retinal vessels stained for ZO-1 (white); scale bar, 50 μm. **Q–R,** Merged images of O-P, ZO-1 (green) and Isolectin (red); scale bar, 50 μm. *Smad6*$^{+/+}$ **(O, Q)** and *Smad6*$^{-/-}$ **(P, R).** *, $P \le 0.05$, **, $P \le 0.01$, ****, $P \le 0.0001$, ns, not significant. Statistical significance in A was determined by one-way ANOVA, and in D, G, J it was assessed using a Student's *t*-test, Mann-Whitney *post-hoc* test, 3 replicates.

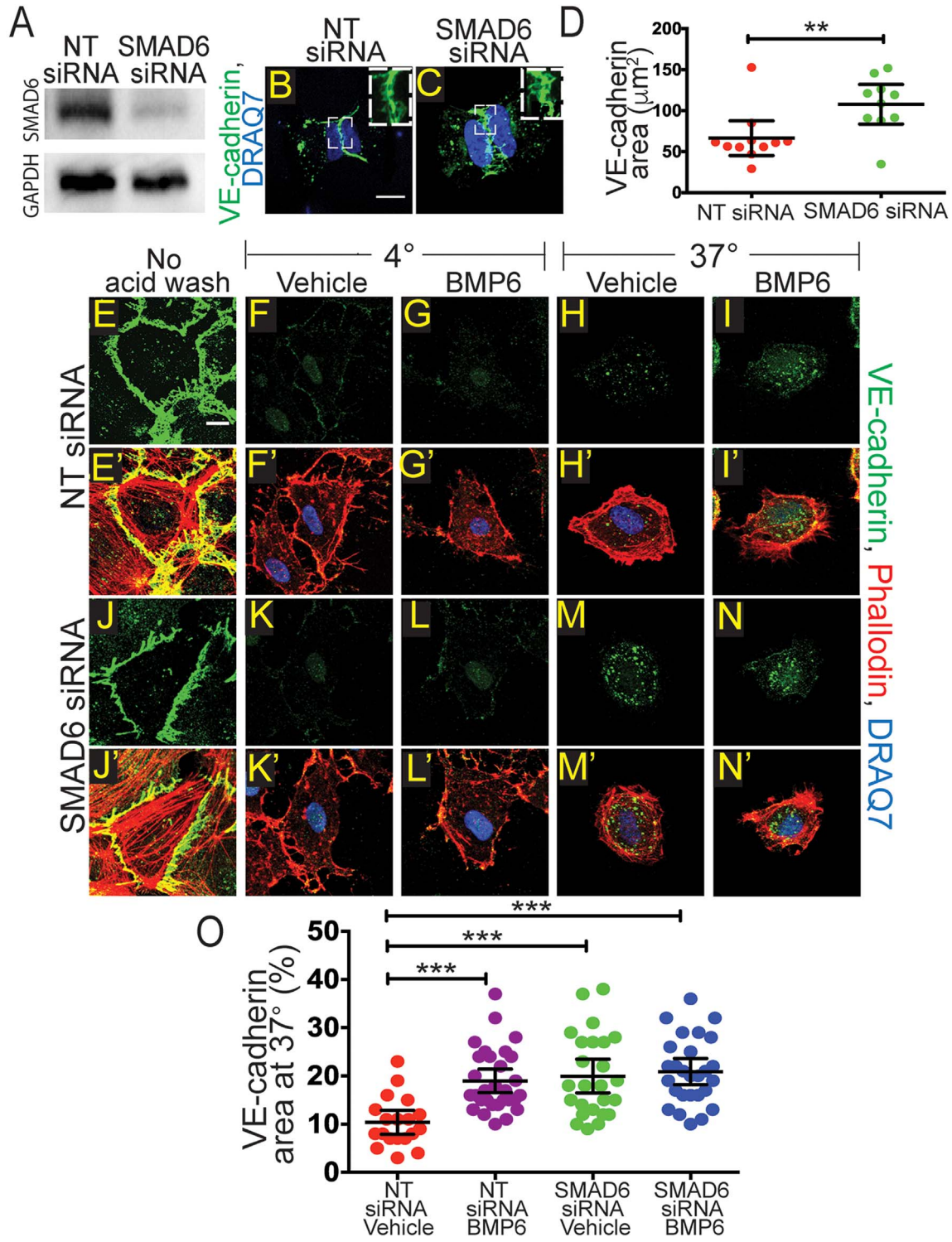


**Fig. 4. Reduced SMAD6 levels promote changes in EC junction morphology and VE-cadherin internalization. A,** Western blot after indicated siRNA treatments. Top, SMAD6 protein; bottom, relative GAPDH. **B–C,** H-micropatterns; scale bar, 10 μm. HUVEC transfected with NT **(B)** or SMAD6 siRNA **(C)** and stained with VE-cadherin (green) to visualize adherens junctions and DRAQ7 (blue) to visualize the nucleus. **D,** Quantification of VE-cadherin area in micropatterns with EC of indicated manipulations. **E–N,** HUVEC internalization assay with indicated treatments after incubation at 4 °C with VE-cadherin antibody; immunofluorescent staining for VE-cadherin (green); scale bar, 10 μm. **E'–N',** Merged images from E–N to include phalloidin (red) and DRAQ7 (blue); scale bar, 10 μm. **E–E',** Control with no acid wash or internalization at 37 °C. **F–F', G–G', K–K', L–L',** Controls kept at 4 °C and acid washed, with or without ligand and with indicated siRNA. **H–H', I–I', M–M', N–N',** HUVEC with or without ligand and indicated siRNA treatment, incubated at 37 °C prior to acid wash. **O,** Quantification of VE-cadherin internalization (% VE-cadherin area normalized to cell area). Statistics, one-way ANOVA with Tukey's *post-hoc* test, *** $P \leq 0.001$; 3 replicates.

likely occurs *via* effects on endothelial cell-cell junctions, as tight and adherens junctions are perturbed in *Smad6* mutant mouse retinal vessels, and adherens junctions in EC with reduced SMAD6 levels. Disruption of EC junctions often results in leakiness of EC monolayers (Orsenigo et al., 2012; Wessel et al., 2014; Hatanaka et al., 2012). Our data is consistent with a model whereby SMAD6 regulates a required switch from a pro-angiogenic phenotype to a quiescent phenotype in arteries during embryogenesis.

BMP signaling is context dependent with diverse responses in EC (Wiley and Jin, 2011). We showed that BMP signaling is repressed in intersegmental vessels that sprout from arteries of zebrafish and active in the caudal vein plexus that sprouts from the axial vein (Wiley et al., 2011). Repressed BMP signaling correlates with Smad6 expression and *Smad6* function in zebrafish arteries (Mouillesseaux et al., 2016). Although SMAD6 is also expressed in nascent heart valves in the mouse (Galvin et al., 2000 and this study), there is no apparent heart valve phenotype or obvious heart defect during embryogenesis in mice lacking *Smad6* function. Instead, mutant embryos have vascular hemorrhage, and this correlates with expression of *Smad6* during development in a subset of arteries, suggesting that blood vessel stability is compromised in the absence of *Smad6*. Another study showed expression of SMAD6 in several areas that sustain cartilage development using an antibody (Estrada et al., 2011), but we were unable to reproduce this expression localization using the *LacZ* reporter. This may result from differences in genetic background or staging. We believe that the vessel hemorrhage phenotype seen in our study is downstream of defects in vessel defects rather than cartilage development.

*Smad6* expression during mouse embryogenesis appears restricted to a subset of vessel arteries that include the dorsal aorta, vertebral arteries, branchial arch arteries and the surface arteries of the brain. It is unclear why these arteries support more expression from the Smad6 locus, while other arteries such as the coronaries show little to no detectable expression at similar developmental stages (data not shown). This could result from environmental cues unique to some but not all arterial beds, or it may reflect different flow parameters affecting the arteries, as SMAD6 expression was reported to be flow-regulated *in vitro* (Topper et al., 1997). Regardless, it is likely that some arteries require SMAD6 to stabilize as they transition from a pro-angiogenic to a quiescent phenotype. How vascular quiescence is achieved is an open question; however, a recent study showed SMAD6 upregulation with aging in primary EC isolated from tissues (Schlereth et al., 2018), suggesting that SMAD6 may be part of a "vascular quiescence" program.

It is notable that amongst the many identified negative regulators of BMP signaling, such as Chordin, Noggin, and Gremlin, most act extracellularly to bind BMP ligand and prevent interaction with BMP receptors (Ali and Brazil, 2014; Walsh et al., 2010; Balemans and Van Hul, 2002). SMAD6 and SMAD7 are among a minority of TGFβ family regulators that act intracellularly to modify signaling responses. SMAD7 inhibits both TGFβ and BMP-induced SMAD signaling, however, SMAD6 preferentially inhibits BMP signaling (Miyazawa and Miyazono, 2017). Interestingly, a BMP regulator that appears to function both intra- and intercellularly, BMPER, is also expressed in the vasculature during development and regulates endothelial barrier function in adult mice (Moser et al., 2003; Helbing et al., 2017). These findings suggest that it is important to regulate the response of endothelial cells and vessels to incoming BMP ligand, and our findings show that *Smad6* function is not redundant with either BMPER or SMAD7 in the developing vasculature.

Examination of postnatal retinal angiogenesis reveals a potential cellular mechanism for the reduced stability of developing vessels *in vivo*. Mice that survived to early post-natal stages and lacked *Smad6* function had increased retinal vascular sprouting and branching, consistent with our previous work showing that SMAD6 is anti-angiogenic in a 3D sprouting model (Mouillesseaux et al., 2016). This exuberant angiogenesis in *Smad6*$^{-/-}$ mutant pups was accompanied by reduced levels of VE-cadherin and ZO-1 localized to cell-cell junctions, although we did not detect obvious hemorrhage, perhaps due to reduced outward pressure or a privileged micro-environment. This suggests that junctions are less stable absent *Smad6* function *in vivo*, and EC with reduced SMAD6 levels revealed increased VE-cadherin internalization *in vitro*, supporting this idea. We showed that SMAD6 negatively regulates BMP signaling in EC, and a recent report showed that BMP signaling decreased EC stability by inducing Src-dependent phosphorylation and internalization of VE-cadherin (Mouillesseaux et al., 2016; Benn et al., 2016). Thus, it is likely that in EC, SMAD6 normally modulates the extent to which VE-cadherin turnover is promoted by BMP signaling. This negative modulation appears to be functionally critical in developing vessels that express SMAD6 to prevent vessel destabilization.

Our work provides compelling evidence that SMAD6 functions to stabilize blood vessels during development, as they transition from an active or pro-angiogenic phenotype to a more quiescent phenotype. Since most adult vessels are quiescent, this finding predicts that *SMAD6* mutations in humans may affect vessel integrity, and *SMAD6* mutations were associated with congenital cardiovascular malformation in recent studies (Gillis et al., 2017; Tan et al., 2012). Taken together, this further understanding of how a negative regulator of BMP signaling, SMAD6, affects angiogenesis and endothelial cell activation in mice reveals critical roles for SMAD6 in both vascular development and homeostasis.

## 4. Materials and methods

### 4.1. Mouse and embryo handling

All experiments involving animals were performed with approval of the UNC-CH IACUC Committee. *Flt1*$^{+/LacZ}$ mice were a gift from Dr. Guo Hua Fong. Generation of *Smad6*$^{-/-}$ mice was previously described (Galvin et al., 2000). *Smad6*$^{+/-}$ embryos were shipped from Dr. Karen Lyons, in agreement with Takeda, Inc., then thawed and injected into pseudo-pregnant females by the Mutant Mouse Resource and Research Center at University of North Carolina. All mice and embryos were on a CD1 background. Embryos of indicated stages were dissected and fixed in 4% paraformaldehyde (PFA) overnight, then stored in phosphate-buffered saline (PBS) at 4 °C. Embryos were embedded in paraffin or OCT and sectioned at 10 μm.

### 4.2. Embryo staining

For whole mount *LacZ* staining, embryos were fixed with glutaraldehyde fix solution (5 mM EGTA, 2 mM $MgCl_2$, 0.2% glutaraldehyde in PBS) for 20 min, washed in X-gal wash buffer (2 mM $MgCl_2$, 0.02% Nonidet P40, in 0.1 M sodium phosphate) and stained for β-galactosidase with X-gal staining solution (5 mM potassium ferrocyanide, 5 mM postassium ferricyanide, 1 mg/mL X-gal in X-gal wash buffer) overnight at 37 °C. *LacZ*-stained whole embryos were embedded in paraffin, sectioned at 10 μm, and counter-stained with Eosin. Hemotoxylin & Eosin and Prussian Blue-DAB staining were performed on paraffin sections according to standard protocols by the UNC Histology Research Core Facility (Fischer et al., 2008; Moos and Mollgard, 1993).

To evaluate *Smad6* expression in vessels, E15.5 embryos were dissected, fixed 1 h at RT in 4% PFA, washed overnight in 30% sucrose, and embedded in OCT the following morning. Serial sections were collected at 10 μm on a Leica CM1860 cryostat and stained with either X-gal overnight at 37 °C after 2 washes in X-gal wash buffer, or antibodies for immunofluorescence. For immunofluorescence on frozen sections, slides were rinsed in PBS, permeabilized for 5 min in 0.2% Triton X-100, blocked in CAS-block (Life Technologies – 00-8120) for 1 h at RT, then incubated in primary antibodies overnight at 1:100 (PECAM, BD Pharmingen – 550274; NG2, Millipore AB5320). The following day, slides were washed in PBS and incubated in 1:100 α-SMA-Cy3 (Sigma C6198), 1:500 Alexa fluor-conjugated secondary antibodies, and 1:100 DAPI for 2 h at RT. Then slides were washed again in PBS and mounted with Prolong Diamond antifade (Life Technologies P36961).

### 4.3. iDISCO and light-sheet imaging

Staged embryos were stained for light-sheet imaging using the iDISCO protocol (including all solutions in protocol) to label large tissues (Renier et al., 2014). Briefly, embryos were fixed overnight in 4% PFA at 4 °C, then washed with PBS and subjected to the non-methanol pretreatment. Embryos were permeabilized for 1 day in permeabilization solution at 37 °C, then blocked in blocking solution for 1 day at 37 °C prior to incubation with PECAM primary antibody (1:20, BD Pharmingen – 550274) in PTwH solution (0.2% Tween-20, 10 µg/µL Heparin in PBS) with 5% DMSO + 3% donkey serum for 2 days at 37 °C. Embryos were washed, incubated in Alexa-fluor-conjugated anti-rat secondary antibody (1:200) in PTwH solution with 3% donkey serum for 2 days at 37 °C, then washed, dehydrated in methanol and cleared by incubating and storing in DiBenzyl Ether at RT. Embryos were imaged on a light-sheet microscope (Ultramicroscope II, LaVision Biotec). Images were processed using Imaris (Bitplane) software.

### 4.4. Quantitative RT-PCR

cDNA was generated from 1 µg mRNA using iScript reverse transcription kit (Bio-Rad 170–8891) and diluted 1:3 in water. qRT–PCR was performed using iTaq Universal SYBR Green SuperMix (Bio-Rad 172–5121). SYBR Green real-time PCR was performed in triplicate on the Applied Biosystems QuantStudio 6 Flex Real-Time PCR System. For quantification, relative expression of each gene to *GAPDH* in each sample was calculated by $2^{(CT \text{ of gene} - CT \text{ of GAPDH})}$. *PECAM*1 was included as a known endothelial marker present in the retina.

### 4.5. Retina acquisition and staining

RNA was collected from retinas dissected immediately after sacrifice by placing them into 500 µL Trizol reagent (Life Technologies 15596026). For immunofluorescent staining, mouse eyes were collected, fixed in 4% PFA for 1 h, dissected and stored in PBS at 4 °C (Powner et al., 2012). Retinas were permeabilized with 0.2% Triton X-100 for 1 h at RT, then blocked with CAS-block for 1 h at RT, followed by overnight incubation with VE-cadherin primary antibody (1:100, Santa Cruz – sc-28644) or ZO-1 (1:100, ThermoFisher 61–7300) at 4 °C. Retinas were washed with PBS, followed by incubation with Alexa fluor-conjugated secondary antibody (1:500) and 488-conjugated Isolectin-IB4 (1:100, Life Technologies – I21411) for 4 h at RT. Retinas were washed in PBS before mounting using Prolong Diamond antifade.

### 4.6. siRNA transfection

HUVEC (Lonza) were transfected with non-targeting siRNA (Life Technologies – 4390847) or SMAD6 siRNA (Life Technologies – 4392420, s8410, s8411) using the standard Lipofectamine 3000 (Invitrogen – L3000008) manufacturer's protocol. Briefly, HUVEC were seeded to be ~70–90% confluent at the time of transfection in EBM-2+EGM-2 BulletKit (Lonza – CC-3156 and CC-3162, respectively). siRNA was diluted in opti-MEM media at 10 nM and incubated for 10 min at RT before adding in Lipofectamine reagent diluted in opti-MEM (1:1 ratio) and incubated for 20 min at RT. The DNA-lipid complex was then added to HUVEC in antibiotic-free media (EBM-2+EGM-2 BulletKit-gentamicin) and incubated overnight at 37 °C. Media was changed the following morning to allow HUVEC to recover and experiments were started 24 h after transfection.

### 4.7. Western blotting

To evaluate knockdown of SMAD6, HUVEC whole-cell lysates were prepared in RIPA buffer supplemented with protease/phosphatase inhibitor cocktail (Cell Signaling 5872S). Lysates were separated on 10% TGX Stain-Free FastCast SDS–PAGE gels (Bio-Rad 161–0183), followed by 1 min ultraviolet activation of TGX stain for total protein quantification. Protein was transferred to polyvinylidene difluoride membranes (Bio-Rad 162–0177), blots were imaged under ultraviolet for total protein, blocked for 1 h in 5% non-fat milk (NFM) in PBS + 0.1% Tween20 (PBST), then incubated overnight at 4 °C with SMAD6 primary antibody (1:5,000, Abcam ab13727) or GAPDH (1:15,000, Cell Signaling 97166S) in 1% NFM in PBST. After washing, horseradish peroxidase-conjugated secondary antibodies (1:15,000, Life Technologies G21234 or 816720) were added for 1 h at RT in 1% NFM in PBST. Luminata Forte (Millipore WBLUF0100) was used for detection. Blots were images on a Bio-Rad ChemiDoc XRS system and band densities were calculated on Bio-Rad Image Lab software, following established guidelines (Gassmann et al., 2009).

### 4.8. Micropatterns

H-pattern chips were purchased from CYTOO Inc. (CYTOO Chips, cytoo.com) and used according to the manufacturer's recommendation. Chips were placed in a 6-well plate and coated with 5 µg/mL fibronectin in PBS for 30 min at 37 °C, then 4 mL of HUVEC resuspended at 15,000 cells/mL were added to each well. Cells were allowed to attach at 37 °C for 20 min before rinsing and addition of new media. To observe 2 cells on a single H-pattern, cells were incubated overnight, then fixed and stained with VE-cadherin and DRAQ7 (to mark the junction and nucleus respectively) using the protocol below for immunofluorescence.

### 4.9. Internalization assay

Internalization assays were performed essentially as described (Carroll et al., 1999; Boucher et al., 2017), with slight modification. For VE-cadherin internalization, HUVEC plated on 0.1% gelatin-coated coverslips and grown to confluency were washed quickly with chilled PBS+ (PBS supplemented with $Ca^{+2}$ and $Mg^{+2}$, ThermoFisher – 14040182) on ice at 4 °C. Following washing, HUVEC were incubated with cold blocking/internalization solution (EBM-2 supplemented with 0.5% w/v BSA) for 30 min on ice at 4 °C. HUVEC were incubated with VE-cadherin BV6 primary antibody (1:100, Enzo – ALX-803-305-C100) in chilled blocking solution for 2 h at 4 °C to label the cell surface pool of VE-cadherin (BV6 binds extracellular domain of VE-cadherin, (Corada et al., 2001)). HUVEC were then washed quickly with cold PBS+ before adding warmed (37 °C) internalization medium (EBM-2 with vehicle or BMP6 treatment) and incubating at 37 °C for 1 h. Control cells were left at 4 °C. HUVEC were then incubated in an acid wash (0.5 NaCl/0.2 M acetic acid in water) for 4 min at 4 °C, washed with PBS, fixed in 4% PFA for 10 min, and stained using the protocol for immunofluorescence.

### 4.10. HUVEC immunofluorescence

HUVEC in micropattern experiments were fixed for 10 min in 4% PFA, washed with PBS, then permeabilized for 20 min in 0.2% Triton X-100. Cells were blocked for 1 h at RT with CAS-block (Life Technologies- 00–8120), then incubated in VE-cadherin primary antibody (1:100, Cell Signaling- D87F2) overnight in CAS-block at 4 °C. Cells were washed in PBS, then incubated with Alexa-fluor-conjugated anti-species secondary antibodies (1:500) plus Alexa-fluor-conjugated phalloidin (1:250, Invitrogen – A12381) and DRAQ7 (1:1000, Abcam – ab109202) in CAS-block for 3 h at RT. For internalization experiments, after VE-cadherin labeling, internalization and subsequent fixation, HUVEC were incubated with Alexa-fluor-conjugated phalloidin (1:250, Invitrogen – A12381) plus Alexa-fluor-conjugated anti-mouse secondary antibody (1:500) and DRAQ7 in CAS-block for 3 h at RT. Coverslips were mounted onto slides using Prolong Diamond antifade and sealed with nail polish.

### 4.11. Imaging

All fluorescent imaging was done using an Olympus FV1200 Laser Scanning Confocal Microscope and Flow View software. All bright field section images were acquired using a Zeiss Imager A2 AX10 microscope and Jenoptik camera.

### 4.12. Statistical analysis

Normalized datasets were graphed and analyzed using PRISM. Chi-square test was used to determine discrepancy between observed and expected numbers of a total of 133 *Smad6*$^{+/+}$, *Smad6*$^{+/-}$, and *Smad6*$^{-/-}$ mice at P0 from *Smad6*$^{+/-}$ intercrosses. To quantify embryo hemorrhage, the number of hemorrhages observed by Prussian Blue-DAB stained E15.5 cross-sections was counted through 1 mm of 10 μm cut paraffin sections. For two-sample data sets with equal variances (control *versus* a single experimental condition) unpaired, two-tailed Student's *t*-test was used along with a Mann-Whitney *post-hoc* test. For data sets with greater than two conditions and equal variances, one-way ANOVA with Tukey's *post-hoc* test was used. * $P \leq 0.05$, ** $P \leq 0.01$, *** $P \leq 0.001$, **** $P \leq 0.0001$, ns, not significant.

All key resources used in experiments are listed in the Key Resources Table.

## Acknowledgments

We thank Bautch lab members for input and constructive discussion. We also thank Michael Zheng, Ariel Gold, and Bianca Rosato for help with genotyping of *Smad6* mice, and Dr. Kathleen Caron for the use of a microscope. We thank Dr. Pablo Ariel from UNC MSL for help with iDISCO staining and light-sheet imaging and Dr. Karen Lyons for sending frozen embryos. We thank Carolyn Suitt for embedding *Smad6* embryos. H & E staining was provided by the Histology Research Core Facility in the Department of Cell Biology and Physiology at the University of North Carolina, Chapel Hill NC.

## Funding

This work was supported by the National Institutes of Health (R01 HL43174 and HL116719, and R35 139950 (VLB)), Integrated Vascular Biology training Grant (T32HL069768), and AHA Predoctoral Fellowship (16PRE29730003 (LAW)).

## Declaration of interests

None.

## Appendix A. Supplementary material

Supplementary data associated with this article can be found in the online version at doi:10.1016/j.ydbio.2018.07.027.

## References

Adams, R.H., Alitalo, K., 2007. Molecular regulation of angiogenesis and lymphangiogenesis. Nat. Rev. Mol. Cell Biol. 8 (6), 464–478.
Ali, I.H.A., Brazil, D.P., 2014. Bone morphogenetic proteins and their antagonists: current and emerging clinical uses. Br. J. Pharmacol. 171 (15), 3620–3632.
Balemans, W., Van Hul, W., 2002. Extracellular regulation of BMP signaling in vertebrates: a cocktail of modulators. Dev. Biol. 250 (2), 231–250.
Benn, A., et al., 2016. VE-cadherin facilitates BMP-induced endothelial cell permeability and signaling. J. Cell Sci. 129 (1), 206–218.
Bentley, K., et al., 2014. The role of differential VE-cadherin dynamics in cell rearrangement during angiogenesis. Nat. Cell Biol. 16 (4), 309–321.
Boucher, J.M., et al., 2017. Dynamic alterations in decoy VEGF receptor-1 stability regulate angiogenesis. Nat. Commun. 8, 15699.
Bragdon, B., et al., 2011. Bone morphogenetic proteins: a critical review. Cell Signal. 23 (4), 609–620.
Cai, J., et al., 2012. BMP signaling in vascular diseases. FEBS Lett. 586 (14), 1993–2002.
Carmeliet, P., 2003. Angiogenesis in health and disease. Nat. Med. 9 (6), 653–660.
Carroll, R.C., et al., 1999. Dynamin-dependent endocytosis of ionotropic glutamate receptors. Proc. Natl. Acad. Sci. USA 96 (24), 14112–14117.
Corada, M., et al., 1999. Vascular endothelial-cadherin is an important determinant of microvascular integrity in vivo. Proc. Natl. Acad. Sci. USA 96 (17), 9815–9820.
Corada, M., et al., 2001. Monoclonal antibodies directed to different regions of vascular endothelial cadherin extracellular domain affect adhesion and clustering of the protein and modulate endothelial permeability. Blood 97 (6), 1679–1684.
Curry, F.R., Adamson, R.H., 2010. Vascular permeability modulation at the cell, microvessel, or whole organ level: towards closing gaps in our knowledge. Cardiovasc. Res. 87 (2), 218–229.
David, L., et al., 2007. Identification of BMP9 and BMP10 as functional activators of the orphan activin receptor-like kinase 1 (ALK1) in endothelial cells. Blood 109 (5), 1953–1961.
David, L., Feige, J.J., Bailly, S., 2009. Emerging role of bone morphogenetic proteins in angiogenesis. Cytokine Growth Factor Rev. 20 (3), 203–212.
Dejana, E., Tournier-Lasserve, E., Weinstein, B.M., 2009. The control of vascular integrity by endothelial cell junctions: molecular basis and pathological implications. Dev. Cell 16 (2), 209–221.
Derynck, R., Zhang, Y.E., 2003. Smad-dependent and Smad-independent pathways in TGF-beta family signalling. Nature 425 (6958), 577–584.
Dorrell, M.I., Aguilar, E., Friedlander, M., 2002. Retinal vascular development is mediated by endothelial filopodia, a preexisting astrocytic template and specific R-cadherin adhesion. Invest. Ophthalmol. Vis. Sci. 43 (11), 3500–3510.
Estrada, K.D., et al., 2011. Smad6 is essential to limit BMP signaling during cartilage development. J. Bone Miner. Res. 26 (10), 2498–2510.
Fischer, A.H., et al., 2008. Hematoxylin and eosin staining of tissue and cell sections. CSH Protoc. 2008, (p. pdb.prot4986).
Fruttiger, M., 2007. Development of the retinal vasculature. Angiogenesis 10 (2), 77–88.
Galvin, K.M., et al., 2000. A role for smad6 in development and homeostasis of the cardiovascular system. Nat. Genet. 24 (2), 171–174.
Gassmann, M., et al., 2009. Quantifying Western blots: pitfalls of densitometry. Electrophoresis 30 (11), 1845–1855.
Gavard, J., Gutkind, J.S., 2006. VEGF controls endothelial-cell permeability by promoting the beta-arrestin-dependent endocytosis of VE-cadherin. Nat. Cell Biol. 8 (11), 1223–1234.
Gerhardt, H., et al., 2003. VEGF guides angiogenic sprouting utilizing endothelial tip cell filopodia. J. Cell Biol. 161 (6), 1163–1177.
Geudens, I., Gerhardt, H., 2011. Coordinating cell behaviour during blood vessel formation. Development 138 (21), 4569–4583.
Giannotta, M., Trani, M., Dejana, E., 2013. VE-cadherin and endothelial adherens junctions: active guardians of vascular integrity. Dev. Cell 26 (5), 441–454.
Gillis, E., et al., 2017. Candidate gene resequencing in a large bicuspid aortic valve-associated thoracic aortic aneurysm cohort: SMAD6 as an important contributor. Front. Physiol. 8, 400.
Hata, A., et al., 1998. Smad6 inhibits BMP/Smad1 signaling by specifically competing with the Smad4 tumor suppressor. Genes Dev. 12 (2), 186–197.
Hatanaka, K., et al., 2012. Fibroblast growth factor signaling potentiates VE-cadherin stability at adherens junctions by regulating SHP2. PLoS One 7 (5), e37600.
Helbing, T., et al., 2017. Bone Morphogenetic protein-modulator BMPER regulates endothelial barrier function. Inflammation 40 (2), 442–453.
Imamura, T., et al., 1997. Smad6 inhibits signalling by the TGF-beta superfamily. Nature 389 (6651), 622–626.
Kametani, Y., Takeichi, M., 2006. Basal-to-apical cadherin flow at cell junctions. Nat. Cell Biol. 9 (1), 92–98.
Komarova, Y.A., et al., 2017. Protein interactions at endothelial junctions and signaling mechanisms regulating endothelial permeability. Circ. Res. 120 (1), 179–206.
Larrivee, B., et al., 2012. ALK1 signaling inhibits angiogenesis by cooperating with the Notch pathway. Dev. Cell 22 (3), 489–500.
Lee, H.-W., et al., 2017. Alk2/ACVR1 and Alk3/BMPR1A provide essential function for bone morphogenetic protein–induced retinal angiogenesis. Arterioscler. Thromb. Vasc. Biol. 37, 657–663.
Miyazawa, K., Miyazono, K., 2017. Regulation of TGF-beta family signaling by inhibitory smads. Cold Spring Harb. Perspect. Biol. 9 (3).
Moos, T., Mollgard, K., 1993. A sensitive post-DAB enhancement technique for demonstration of iron in the central nervous system. Histochemistry 99 (6), 471–475.
Moser, M., et al., 2003. BMPER, a novel endothelial cell precursor-derived protein, antagonizes bone morphogenetic protein signaling and endothelial cell differentiation. Mol. Cell. Biol. 23 (16), 5664–5679.
Mouillesseaux, K.P., et al., 2016. Notch regulates BMP responsiveness and lateral branching in vessel networks via SMAD6. Nat. Commun. 7, 13247.
Orsenigo, F., et al., 2012. Phosphorylation of VE-cadherin is modulated by haemodynamic forces and contributes to the regulation of vascular permeability in vivo. Nat. Commun. 3, 1208.
Powner, M.B., et al., 2012. Visualization of gene expression in whole mouse retina by in situ hybridization. Nat. Protoc. 7 (6), 1086–1096.
Renier, N., et al., 2014. iDISCO: a simple, rapid method to immunolabel large tissue samples for volume imaging. Cell 159 (4), 896–910.
Ricard, N., et al., 2012. BMP9 and BMP10 are critical for postnatal retinal vascular remodeling. Blood 119 (25), 6162–6171.
Risau, W., 1997. Mechanisms of angiogenesis. Nature 386 (6626), 671–674.
Schlereth, K., et al., 2018. The transcriptomic and epigenetic map of vascular quiescence in the continuous lung endothelium. Elife 7.
Shi, Y., Massague, J., 2003. Mechanisms of TGF-beta signaling from cell membrane to the nucleus. Cell 113 (6), 685–700.

Smith, W.C., 1999. TGF beta inhibitors. New and unexpected requirements in vertebrate development. Trends Genet. 15 (1), 3–5.
Tan, H.L., et al., 2012. Nonsynonymous variants in the SMAD6 gene predispose to congenital cardiovascular malformation. Hum. Mutat. 33 (4), 720–727.
Topper, J.N., et al., 1997. Vascular MADs: two novel MAD-related genes selectively inducible by flow in human vascular endothelium. Proc. Natl. Acad. Sci. USA 94 (17), 9314–9319.
Tseng, Q., et al., 2012. Spatial organization of the extracellular matrix regulates cell-cell junction positioning. Proc. Natl. Acad. Sci. USA 109 (5), 1506–1511.
Vestweber, D., et al., 2009. Cell adhesion dynamics at endothelial junctions: VE-cadherin as a major player. Trends Cell Biol. 19 (1), 8–15.
Wallez, Y., Huber, P., 2008. Endothelial adherens and tight junctions in vascular homeostasis, inflammation and angiogenesis. Biochim. Biophys. Acta 1778 (3), 794–809.
Walsh, D.W., et al., 2010. Extracellular BMP-antagonist regulation in development and disease: tied up in knots. Trends Cell Biol. 20 (5), 244–256.
Wessel, F., et al., 2014. Leukocyte extravasation and vascular permeability are each controlled in vivo by different tyrosine residues of VE-cadherin. Nat. Immunol. 15 (3), 223–230.
Wiley, D.M., et al., 2011. Distinct signalling pathways regulate sprouting angiogenesis from the dorsal aorta and the axial vein. Nat. Cell Biol. 13 (6), 686–692.
Wiley, D.M., Jin, S.-W., 2011. Bone morphogenetic protein functions as a context-dependent angiogenic cue in vertebrates. Semin. Cell Dev. Biol. 22 (9), 1012–1018.